Tuning the thermal stability of copper(II) hexacyanoferrate(II)

Micheal P Moloney, Nicolas Massoni, Agnès Grandjean

Tuning the thermal stability of Copper (II) Hexacyanoferrate(II) nanoparticles

Mícheál P Moloney, [†¥] Nicolas Massoni, [†] Agnès Grandjean[¥]

[†] CEA, DEN, Univ. Montpellier, DE2D, SEAD, Laboratory of Supercritical and Decontamination Processes, , F-30207 Bagnols-sur-Cèze, France

[¥] CEA, DEN, Univ. Montpellier, DE2D, SEVT, Research Laboratory for the development of conditioning matrices, F-30207 Bagnols-sur-Cèze, France

Abstract

It is well known that the physical properties of nanoparticles can be tuned by controlling synthetic factors such as pH, temperature, reactant ratio or type of stabiliser used. In this work the reactant ratio is varied to produce batches of Copper (II) Hexacyanoferrate (II) (Cu-HCF) with different cyano decomposition temperatures. This is accomplished by controlling the number of $Fe(CN)_6^{4-}$ site vacancies throughout the structure. By reducing the number of vacancies, and consequently the need for water to complete the structure, the thermal decomposition temperature of Cu-HCF can be increased. In addition to this we also note that the guest ion similarly contributes to the decomposition temperature. By exchanging K^+ with Cs^+ an increased resistance to thermal decomposition is realised. As the incorporation of Cs^+ ions into the structure does not alter the number of $Fe(CN)_6^{4-}$ site vacancies this enhancement is attributed to a change in the geometry of the copper co-ordination sphere.

Introduction

Hexacyanoferrates (HCFs) of various transition metals have once again begun to attract attention as sorbents in the selective extraction of Cs^+ ions.[1,2,3,4,5,6,7,8,9,10] This is due to their high sorption capacity for caesium over a wide pH range, in high salinity, and their high stability.[11,12,13,14,15] In case of K-Hexacyanoferrates of transition metals, and especially Cu-HCF, the Cs^+ sorption mechanism occurs via an ionic exchange between K^+ from the solid structure and Cs^+ from the solution.[16] Although polynuclear supramolecular complexes these materials can also be classified as nanoparticles, (**Figure 1**).[17,18] It is well recorded in the

literature that in the nanodomain, materials begin to exhibit unique properties, due in some cases to their size and in others to their high surface area to mass ratio.[19,20] Understanding and controlling these properties is vital to engineering nanomaterials with the desired properties. Particle properties can be tuned by controlling experimental factors such as the pH, temperature, type of stabiliser used, or even reactant ratio during synthesis. [21,22,23] For example by varying the metal to non-metal ratio in luminescent quantum dots it is possible to tune both their size and quantum yield.[24] In this work we propose to use one of the aforementioned techniques (reactant ratio) to determine if it is possible to tune the physical properties (thermal resistance) of Cu-HCF. It is well known that it is possible to produce Cu-HCF with varied Cu, Fe, H_2O and K content.[7] Here, we report that by controlling the Cu:Fe ratio we tune the amount of structural water present in each batch, this in turn affects the thermal stability of the cyano ligands. Finally by exchanging the guest ion, K^+ for Cs^+, it was possible to further increase the thermal stability of the cyano ligand. This was attributed to the decreased interaction of the Cs^+ guest ions with the structural water.
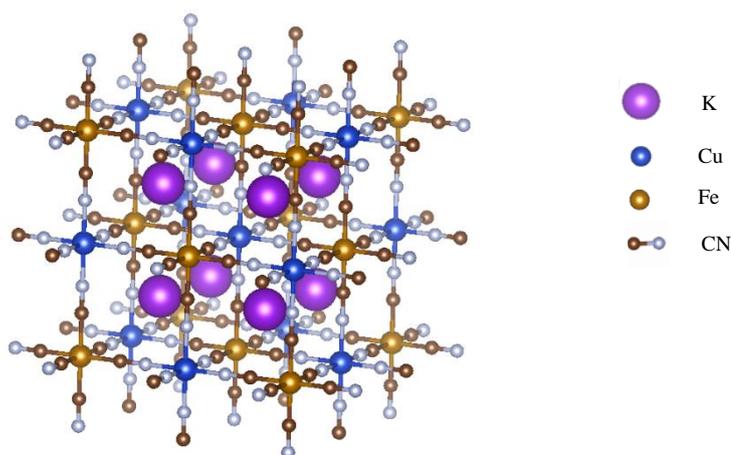

Figure 1: Schematic representation of the structure of $K_2CuFe(CN)_6$ in which none of the Fe sites are vacant.

In this work, five separate batches of Cu-HCF (II) were prepared by a simple co-precipitation reaction that gives nanoparticles as previously reported.[9] Each batch contained a different ratio of Cu^{2+} to $Fe(CN)_6^{4-}$ ions at moment of contact (i.e. before co-precipitation). Batch 1 was prepared using an initial 0.5:1 ratio of Cu^{2+} to $Fe(CN)_6^{4-}$, this was increased to 1:1, 1.5:1, 2:1 and 2.5:1 for batches 2, 3, 4 and 5 respectively. Elemental analysis (EA) and TGA of the final products confirmed different Cu to Fe ratios as well as K and water content, (**Table 1**). Interestingly, it was also found that despite 5 different initial reactant ratios being used only three distinct particle stoichiometries were created. This suggests that there are preferred

stoichiometries. FT-IR and XRD demonstrated that as we move across the 3 stoichiometries the material is consistently copper (II) hexacyanoferrate (II) with no changes in the oxidation state being observed. However, these techniques were used in conjunction with each other to highlight the (re)arranging of the $Fe(CN)_6^{4-}$ vacancies as well as changes in the local Cu chemical environments as the copper ratio was increased. Finally, TGA and FT-IR were used to show an increase in the thermal stability of the CN ligand as the copper to iron ratio approached 1:1. We believe that this is due to a dependence on the quantity of structural water within the material. That is, as the number of Fe vacancies (and therefore number of moles of structural water) are decreased, the higher the thermal stability of the material will be. Finally, the replacement of K^+ with Cs^+ as the guest ion caused a further increase in the thermal stability of the material. While Cs^+ sorption does not affect the amount of structural water it does cause a change in the copper co-ordination sphere as noted by FT-IR. It is assumed that the Cs^+ (as with K^+) guest ions interact with the structural water partially sharing it with the copper.[25] By replacing K^+ with an ion which does not interact as strongly with water this allows for a strengthening/shortening of the $Cu-OH_2$ bond.[26,27]

Experimental

$K_4[Fe(CN)_6].3H_2O$, $CsNO_3$ and $Cu(NO_3)_2.3H_2O$ were purchased from Sigma-Aldrich. Millipore water was used in the synthesis of the Copper (II) Hexacyanoferrate (II) particles.

Copper (II) Hexacyanoferrate (II), here on referred to as Cu-HCF (II), was prepared by the direct addition of a volume (V1) of an aqueous (Millipore) 1.5×10^{-1} M $Cu(NO_3)_2.3H_2O$ solution to a fixed volume (V2) of a 1×10^{-1} M aqueous solution of $K_4[Fe(CN)_6].3H_2O$ (K-HCF). The Cu:Fe ratio was controlled by modifying the ratio V1 to V2. Five batches in total were produced with an initial Cu to Fe ratio of i). 0.5:1, ii). 1:1, iii). 1.5:1, iv). 2:1 and v). 2.5:1. Upon addition of the blue coloured copper solution to the light yellow K-HCF solution a dark burgundy coloured precipitate was immediately formed. The contents of the reaction vessel were then allowed to mix for an hour by rotary mixing. The resulting solid was then collected by centrifugation and washed several times with Millipore water. As the washing steps accumulate, batches 1 and 2 become more and more stable in water and therefore acetone (50% v/v) was needed as a non-solvent to help crash out the particles. This is assumed to be because of the majority presence of $Fe(CN)_6$ groups on their surfaces.[28] Once the washing steps are complete (4 washes) the Cu-HCF was dried under rotary evaporation at 60 ^{0}C. The resulting

dark solid was then examined using Elemental Analysis (EA), DLS, FT-IR, TGA, and XRD. As it is possible to monitor the concentration of $K_4Fe(CN)_6$ and $Cu(NO_3)_2$ in solution via UV-Vis active the supernatant of each batch was examined by UV-Vis after the particles were removed.

Chemical compositions were measured by inductively coupled mass spectrometry for Cu, Fe, K, (and Cs for exchanged sample) after particles were dissolved via microwave radiation in HNO_3. Water content was determined using TGA. It has been shown that TGA results for HCF's can vary with heat rate, mass of sample, or even the type of crucible used.[29] Therefore, when examining the samples in this work all three aforementioned factors were kept constant. TGA experiments were taken between 30 -300°C in air at a heating rate of 30 ^{0}C/min, using a Mettler Toledo TGA/DSC 1 star^e system. Sample mass was kept constant at 20 mg. Crucibles did not have lids placed on them.

The crystalline structure was identified using powder XRD which were performed using a Panalytical X'Pert MPD Pro spectrometer in a Bragg-Brentano geometry. A copper tube (λ=1,5406Å) with a nickel filter was used with an X'Célérator detector. Typical measurement was completed in 5h between 10 and 90°2θ. The X-Ray refinements were profile matching done with the Fullprof freeware included in the Toolbar Fullprof Suite V. July-2017.

Chemical structure was studied using FT-IR. The measurements were carried out using a Nicolet iS50.

Zetapotential and size measurements were carried out in water using a Malvern Nano ZS.

Thermal behaviour was also followed using FT-IR. Each batch was taken and placed in an oven where it was heated in air to the desired temperature and allowed to stand at this temperature for 4 hours before being cooled and examined by FT-IR.

K/Cs exchanges were conducted using a high concentration Cs solution (700mg/L Cs; source $CsNO_3$). Each experiment consisted of contacting 100 mg of dried samples with 100 mL of the above mentioned solution. Langmuir Isotherms (**SI**) confirmed this concentration was sufficient for each batch to reach its respective Cs capacity.

Results and discussion

1. Chemical Composition

Elemental analysis (EA) and TGA were used to determine if changing the ratio of $Cu(NO_3)_2$ to $K_4Fe(CN)_6$ would alter the actual particle stoichiometry, including guest ion and water content. These techniques were vital as they allowed for the ascertainment of the exact degree of vacancies, and consequently the H_2O and K content within the particles. The results of these analyses are displayed in **table 1**. [Oxidation numbers for each compound reported on table 1 do not amount to zero. However, this 2-4% discrepancy falls well within the elemental analysis 10% margin of error.] The most striking result is the enforcement of what appears to be three distinct population types throughout the series.

<u>Batches 1 and 2</u> produce almost identical results with 1.27 ± 0.01 Cu for every Fe. Both of these results show a considerably higher Cu to Fe ratio than the initial reactant ratio. This ratio seems to be desired as UV-Vis of the supernatants confirmed that $K_4Fe(CN)_6$ was still available to both batches.

<u>Batch 3</u> is composed of Cu-HCF particles with a final ratio of 1.66 Cu to every 1 Fe. [Considering there is a 10% error in the EA analysis this final stoichiometry is very close to that of the reactant ratio of 1.5:1.] UV-Vis shows no $Fe(CN)_6$ or $Cu(NO_3)_2$ present in the supernatant.

<u>Batches 4 and 5</u> both show 1.9 Cu's for every Fe. This is in good agreement for batch 4's reactant ratio of 2:1 but not batch 5's, this indicates that we have reached max Cu^{2+} to $Fe(CN)_6^{4}$.

Table 1: ICP-MS: moles of Cu, K and Fe in all 5 batches, water content was calculated from TGA results. Data has been normalised with respect to Fe. Note: * (Cu to Fe reactant ratio), §(Cu to Fe ratio in final product).

Batches	Cu:Fe*	Cu§	Fe§	K§	Formula
1	0.5:1	1.26	1	1.69	$K_{1.69}Cu_{1.26}Fe(CN)_6.1.3H_2O$
2	1:1	1.28	1	1.60	$K_{1.6}Cu_{1.28}Fe(CN)_6.1.3H_2O$
3	1.5:1	1.66	1	0.82	$K_{0.82}Cu_{1.66}Fe(CN)_6.3.7H_2O$
4	2:1	1.90	1	0.34	$K_{0.34}Cu_{1.9}Fe(CN)_6.5.4H_2O$
5	2.5:1	1.90	1	0.33	$K_{0.33}Cu_{1.9}Fe(CN)_6.5.4H_2O$

The aforementioned preparations were repeated multiple times to confirm the results. The fact that no batch resulted in a 1:1 ratio of Cu to Fe(CN)$_6$ indicates that the presence of a certain number of Fe(CN)$_6$ vacancies seems to be energetically desirable. These results suggest a minimum (1.3:1) and maximum (1.9:1) Cu^{2+} to Fe(CN)$_6$$^{4-}$ range in which stable Cu-HCF particles can be produced.

EA also showed that the K concentration decreased as Cu increased. This is understandable as the guest K$^+$ ions act as charge balancers in this material. As the ratio of the cationic Cu^{2+} to anionic Fe$_{(II)}$(CN)$_6$$^{-4}$ is increased, the need for cationic K$^+$ will be reduced. Finally, the water content was calculated using TGA. It showed that as the copper content increased so too did the water content. This is also understandable as water is used to complete coppers co-ordination sphere when cyano ligands are unavailable. TGA showed the water content to be 5%, 15.4% and 20% (weight %) for batches 2, 3 and 4 respectively. Combining this with the previously discussed elemental analysis data it gives the structural formulas K$_{1.6}$Cu$_{1.28}$Fe(CN)$_6$.1.3H$_2$O - (type I) , K$_{0.82}$Cu$_{1.66}$Fe(CN)$_6$.3.7H$_2$O - (type II) and K$_{0.34}$Cu$_{1.9}$Fe(CN)$_6$.5.4H$_2$O – (type III) respectively (**Table 1**). From this point on, for simplicities sake, only batches 2, 3 and 4 will be examined as they represent the three population types.

2. Structural properties of Cu-HCF types

XRD

XRD of the three types (batches 2, 3 and 4) showed that they all possessed an F-centred cubic unit cell, (**Figure 2**).[30] Rietveld refinement showed that the lattice constants were a=10.0421 ± 0.0175Å, a=10.0039 ± 0.0040 Å and a=10.0007 ± 0.0042 respectively. This decrease in size could be due to the decrease in K$^+$ content as seen in the elemental analysis,[7] or perhaps it might also be a result of the increased copper content enhancing the already strong copper cyano back bonding effect.[31,32] While the three XRDs scans are quite similar there are slight differences which are clearly visible between each batch. These differences are small, quite broad, additional reflections in batches 3 and 4 at 12.5°, 20°, 21.5° and 26.5° which do not belong to the Bragg reflections of the Fm3m space group. It was found that a Pm3m cubic fit worked better here. As Jiménez-Gallegos et al[33] pointed out, when closely examining the structure of cubic hexacyanoferrates their vacancy distribution is normally random and therefore the

structure can be assigned to a Fm3m structural model. However, as the vacancies begin to become more organised a Pm3m model is a more accurate fit (**Figure 2**).[33]

It should also be noted that in the case of the Fm3m space group, copper is assigned a single chemical environment of $Cu(NC)_4(OH_2)_2$. Conversely, in the Pm3m fit Cu is assumed to have several environments. (This point will be raised again in the FT-IR section.) Finally, the reflections in batches 3 and 4 are narrower when compared to batch 2; the narrowing of the peaks indicates an increase in sample crystallinity.

Therefore, moving from type I (batch 2) to type III (batch 4), as the Cu:Fe ratio is increased the Fe vacancy distribution becomes less random and several Cu environments are created. There is also an increase in the crystallinity.
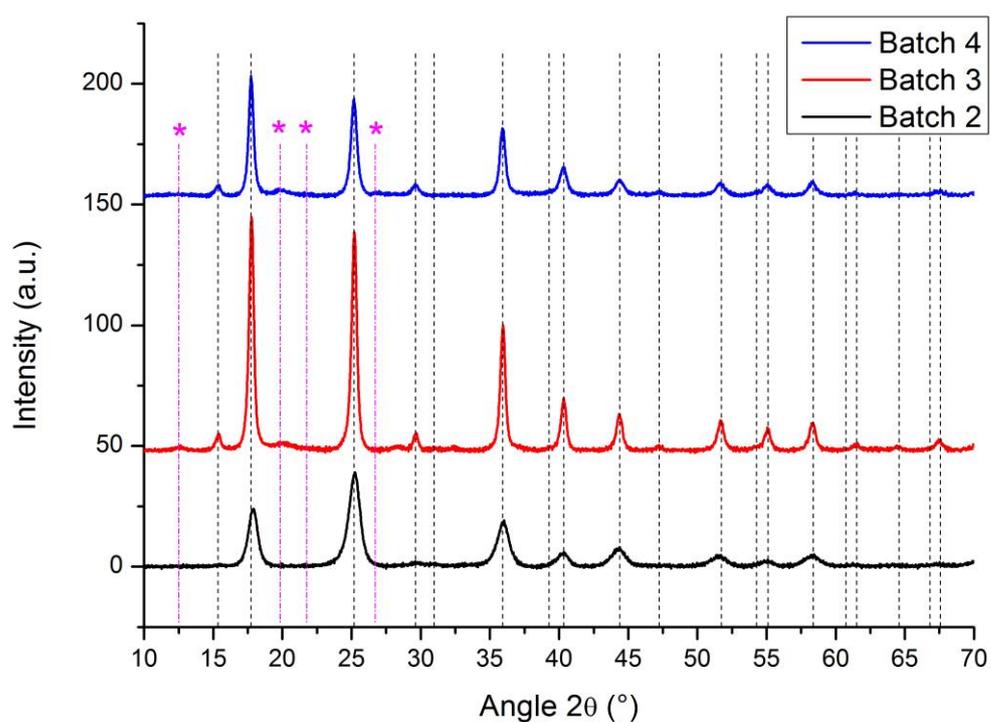

Figure 2: XRD of batches 2 (black), 3 (red) and 4 (green). The black dotted vertical lines are the Bragg reflections for a Fm3m space group. The purple vertical lines indicated with an asterisk are respectively the 1st, 4th, 5th and 7th supplementary Bragg reflections from a Pm3m space group (remaining reflections were either superimposed with the Fm3m ones or omitted for clarity)

FT-IR

In the FT-IR spectra of transition metal hexacyanoferrates (HCF's) three regions are concentrated on. These are i). the M-L region between 400 cm^{-1} - 900 cm^{-1}, ii). the v(CN) region from 1,900 cm^{-1} - 2,200 cm^{-1}, and finally iii). two separate water regions one between 1,500 cm^{-1} - 1,700 cm^{-1} and the second between 3,000 cm^{-1} to 4,000 cm^{-1}.[32, 34,35,] The exact position of these peaks, especially the very prominent v(CN) stretch, is dependent on a). the type of metals present and b). their oxidation state(s). The sensitivity of these peaks to their local environment therefore makes FT-IR an invaluable tool when characterising these compounds.[36]

v(CN) region from 1,900 cm-1 - 2,200 cm-1

Generally speaking, for Cu-HCF (II) the v(CN) stretch can be found at around 2,080 cm^{-1}, with an increase in frequency to 2,180 cm^{-1} if the HCF iron is oxidised from Fe$^{(II)}$ to Fe$^{(III)}$.[31, 35] As the v(CN) of all samples remains around 2,080 $\pm$ 10 cm^{-1} we can say with a fair amount of certainty that throughout the series of experiments Fe remains in the (II) oxidation state (**Figure 3**).

The v(CN) of batch 2 is recorded at 2,070 cm^{-1}. This shifts to 2,090 cm^{-1} and 2,091 cm^{-1} for batch 3 and 4 respectively. This increase in energy indicates a strengthening of the cyano bonds. Cu^{2+} has the ability to fill its 3d shell by receiving electrons from the CN's 5σ orbital.[32] These bonds are further strengthened by the cyano's ability to accept electrons from the copper in a back donation via a π bond into the cyano's anti-bonding π-orbital.[31] By increasing the number of coppers relative to the numbers of cyano ligands we increase the back donated electron density, this in turn strengthens the cyano bond and causes the v(CN) to increase in frequency.

M-L region between 400 cm^{-1} to 900 cm^{-1}

Looking to the M-L region the v(Fe-C) stretch, was recorded at 590 cm^{-1}, 594 cm^{-1}, 593cm^{-1} respectively for batch 2, 3 and 4. This is in good agreement for Cu-HCF (II), as its v(Fe-C) is normally seen at around 595 cm^{-1}, (**Figure 3 - Inset II**).[35]

While this is all noteworthy a more drastic change takes place when looking at the second signal(s) in the M-L region, the v(Cu-N). Depending on the copper to iron ratio this peak can appear as either a broad singlet, or well-structured doublet. This splitting of the v(Cu-N) peak can be explained by the presence of a Jahn-Teller tetragonal distortion within the Cu octahedral.[37] Looking to **Figure 3** we would tend to agree with this assignment, especially as the presence of the second peak becomes more and more evident as the copper to iron ratio is increased. This is in good agreement with what was previously seen in the XRD, i.e. the

creation/enhancement of a second Cu environment. Starting with Batch 2 the v(Cu-N) is seen as a broad peak at 472 cm^{-1} with a partially hidden shoulder at 488 cm^{-1} (**Figure 3 - Inset II**). As the copper ratio is increased the shoulder (now at 494 cm^{-1}) becomes more structured and increases in strength. This shows that a). multiple copper environments are present, and b). that they are dependent on the Fe:Cu ratio.
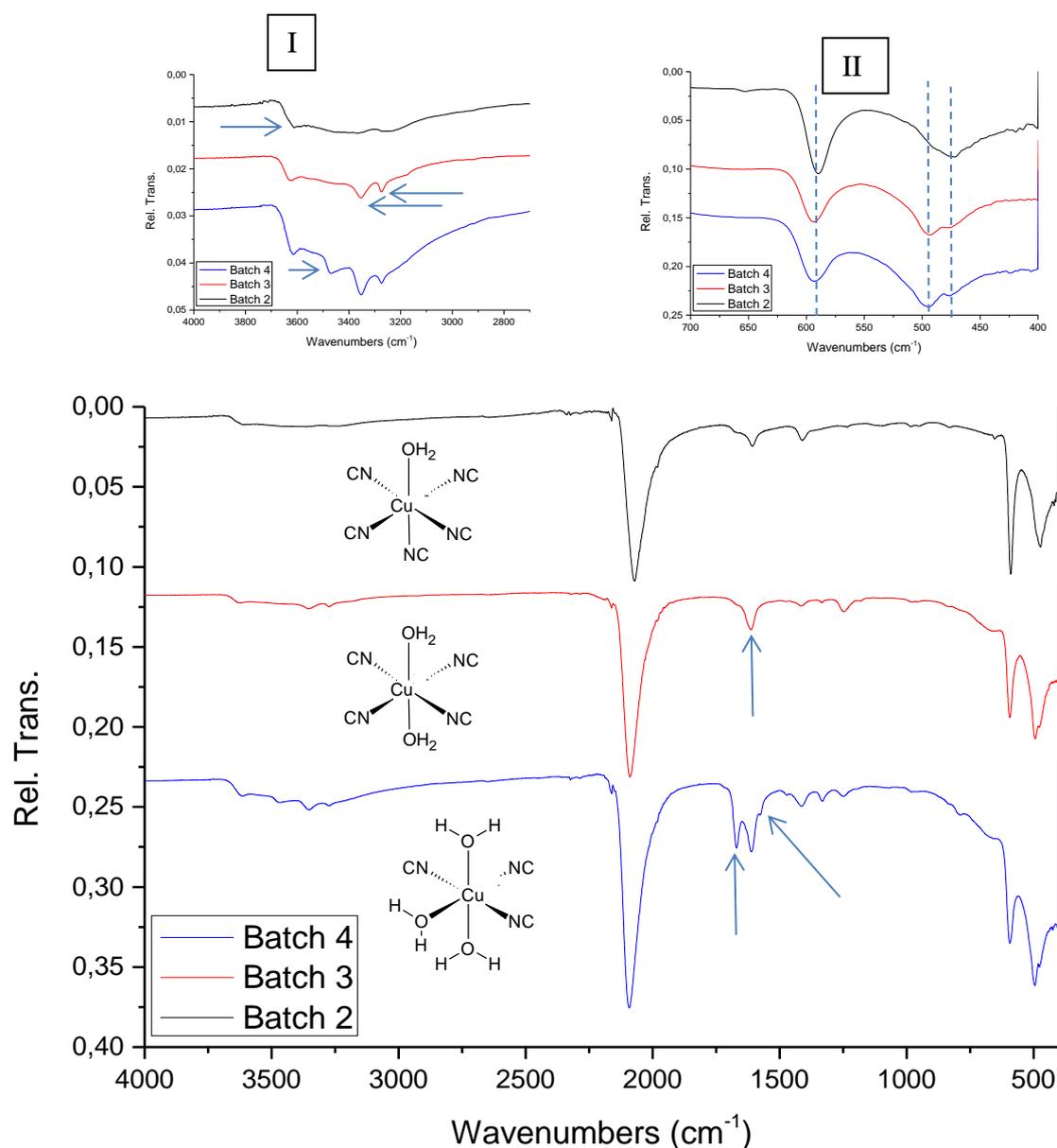

Figure 3: FT-IR of batches 2 (black), 3 (red) and 4 (blue) Cu-HCF. Note the increase in the number of co-ordinated water peaks as the copper to iron ratio is increased.

Water Signals

This assessment (multi-copper environment) is supported when looking at the water regions of the spectra. HCF's possess two types of water, structural (co-ordinated water) and zeolithic (non-structural water molecules present in the pores). Structural water is H_2O which is co-ordinated to the hetero-metal (in this case copper) centres of the structure. These molecules are needed to complete the crystal unit where one or more of the $Fe(CN)_6^{4-}$ units are missing. It is for this reason that they are referred to as structural water. FT-IR can distinguish between structural and zeolithic water. Coordinated (structural) water can be identified by the presence of well-structured peaks, the $\delta(HOH)$ stretches found between 1600 cm^{-1} - 1700 cm^{-1}, and the $\nu(OH)$ stretches between 3,500 cm^{-1} to 4,000 cm^{-1}. The second type of water (zeolithic) is not structural and can be considered to be "free", or more likely, loosely bound through hydrogen bonding to any crystalline water present nearby. However, these bonds are relatively weak and therefore this type of water is usually characterised by the presence of a broad hump like structure between 3,000 cm^{-1} to 3,500 cm^{-1}.

As shown in **Figure 3**, FT-IR of batch 2 displays a $\delta(HOH)$ peak and shoulder at 1600 cm^{-1} and 1,660 cm^{-1} respectively. As the copper ratio is increased the shoulder at 1,660 cm^{-1} continues to grow and sharpen eventually becoming a peak in batch 4, (**Figure 3**). Batch 4 also displays a third $\delta(HOH)$ water peak beginning to appear at 1,576 cm^{-1}. the $\nu(OH)$ region shows for batch 2 a single relatively well-structured coordinated $\nu(OH)$ peak at 3,565 cm^{-1} with two broad hump-like peaks present nearby at 3,402 cm^{-1} and 3,240 cm^{-1}, are also seen, (**Figure 3 - Inset I**). In batch 3 we see that is now consists of three distinct peaks with a forth added in batch 4. In all cases, the zeolithic humps are still visible, though diminished, (**Figure 3 - Inset I**). All of this demonstrates not only an increase in the type of co-ordinated water as we increase the Cu to Fe ratio but also an increase in the number of co-ordinated water environments.

Inset in Figure 3 show the representations of each batches average $Cu(NC)_x(OH_2)_y$ copper coordination sphere to the closet whole number. According to EA copper in batches 2, 3 and 4 will have 4.8, 3.6 and 3.1 cyano ligands respectively. The remaining spots in the octahedron are occupied by water molecules.

DLS

Zeta potential measurements of batches 2, 3 and 4 showed the surface charge of each batch to be -45.4 mV, -31.7 mV and -27.7 mV respectively, (**Figure 4**). The greater surface negativity

of batch 2 suggests a surface less dominated by hydrated copper than batches 3 or 4. This is also reflected in the aggregate sizes, where increased amounts of surface cyano aid in particle dispersion.[9] The reduction in surface charge as the Cu:Fe ratio increased is believed to be due to the greater presence of hydrated Cu (as opposed to cyano groups) on the particles surfaces as we move from batch 2 to 4.
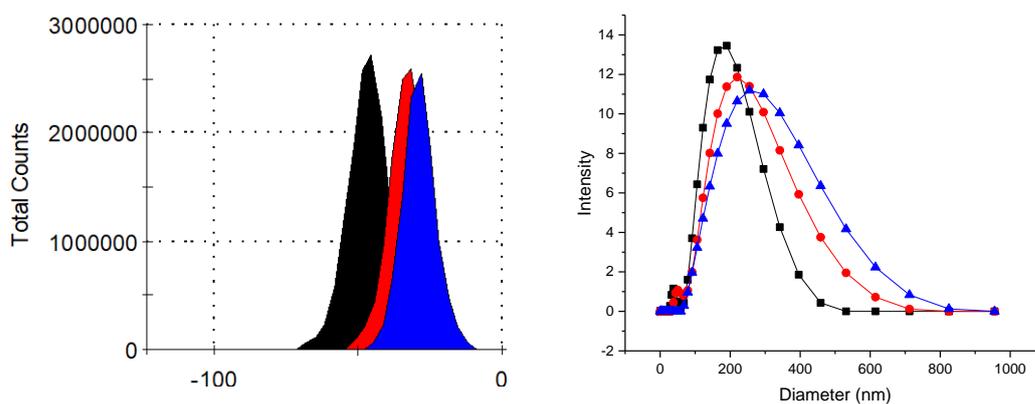

Figure 4: Zeta Potential (left) and size (right) measurements of each batch measured in mV and nm respectively.

Structural Conclusions

Elemental analysis showed an increase in the number of $[Fe(CN)_6]^{4-}$ site vacancies as the copper to iron ratio was increased. XRD while identifying each batch as cubic Cu-HCF, also showed that as the copper content was increased the $[Fe(CN)_6]^{4-}$ site vacancies within the structure began to organise leading to the creation of multiple copper environments. As Jiménez-Gallegos et al. pointed out, in a random distribution of vacancies the structure is assigned the Fm3m structural model and all copper sites are equivalent, with each copper possessing four CN ligands plus two water molecules, $Cu(NC)_4(H_2O)_2$. However, in an ordered vacancy distribution, the 1b and 3d sites have different occupation factors and this leads to different coordination environments for the copper atom. FT-IR confirmed this showing the v(Cu-N) stretch as a broad singlet at low copper concentration (batch 2) which then split into a discernible doublet as the copper to iron ratio was increased, **(Figure 3 – Inset II).** FT-IR also showed the simultaneous appearance of new well defined co-ordinated water peaks again indicating new copper environments being formed. Recalculating the copper to iron ratio where Cu equals 1, we find that the three batches have a Cu to Fe ratio of 1:0.8, 1:0.6 and 1:0.5. Therefore, we can view the three batches of Cu-HCF produced here as having either 20%, 40% or 50% of their $Fe(CN)_6$ units "missing". If the Cu-HCF structure is pictured as a 3-dimensional

cage of ever repeating Cu-N-C-Fe units (**Figure 1**) where each Fe atom supplies 6 CN ligands, it stands that when a Fe is missing the corresponding 6 CN ligands will also be missing. The coordination sphere of any adjacent copper is then completed with water ligands. The more iron sites which are vacant the higher the dependency on water to complete the structure, (**Figure 5**). Finally, DLS showed that the Fe vacancies are not just internal but are present on the particles surface as well. As the Cu:Fe ratio is increased the particles surfaces becoming more neutral as the ratio of Fe-CN$^-$ to Cu-OH$_2$ surface groups decreases.

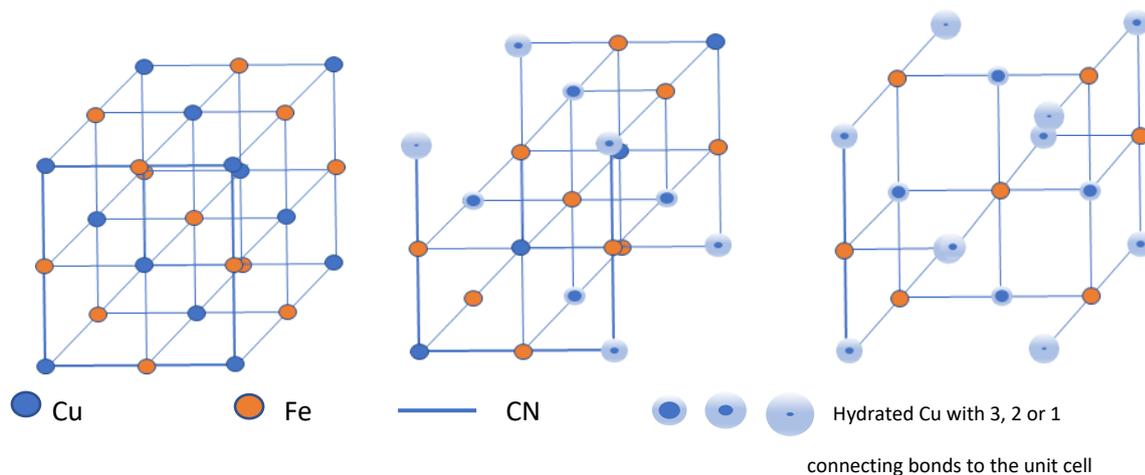Cu   Fe   —— CN   Hydrated Cu with 3, 2 or 1 connecting bonds to the unit cell

Figure 5: From left to right Cu-HCF with 0, 20, and 50 % of the Fe(CN)$_6^{4-}$ sites vacant. As the number of vacancies increase the materials dependence on water to complete the structure increases.

3. Link between thermal stability and Cu-HCF type

Each batch was examined in air between 30-300 ^{0}C, **Figure 6**. This temperature range was chosen to allow us to more closely monitor water loss, and with it the eventual decomposition of the CN ligand. All three samples show mass loss from 60 - 120-125 °C and a distinctive shoulder between 150 - 200 ^{0}C There is however, a notable difference is the position of the shoulder between batch 2 and batches 3/4. While it is at around 170 ± 4 ^{0}C for batches 3 and 4 it is 197 ^{0}C for batch 2. [Note: The total degree of mass loss across the temperature range is quite different for all three batches; however, this can be explained by the difference in particle stoichiometry across the series.] Finally, while batches 3 and 4 show a mass gain step at around 250 ^{0}C (indicating oxidation), batch 2 does not.   Looking at the DSC, (**Figure 6 – Inset**), we see a number of distinct exothermic peaks corresponding to mass loss (or gains) between 90 ^{0}C

and 260 ^{0}C in batches 3 and 4, while batch 2 shows only a rising diagonal line with little fine structure.

To more fully understand these results and to attribute each mass loss and shoulder to water loss and/or cyano decomposition, the samples were heating to certain temperatures within the above range and examined using FT-IR.
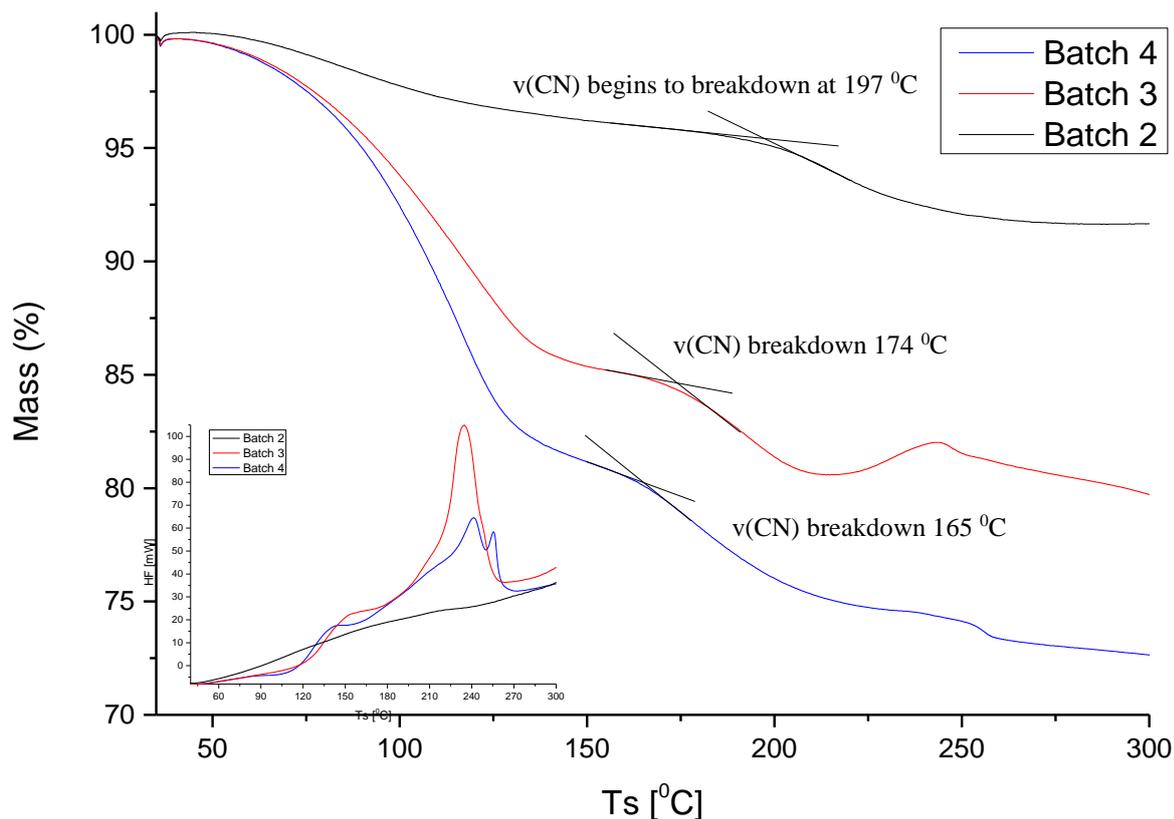

Figure 6: TGA and DSC (inset) of batches 2 (blue), 3 (green) and 4 (red) Cu-HCF.

Each batch was firstly heated to 140 ^{0}C for 4 hours (2 ^{0}C/min) in air. This process was continued jumping 10 ^{0}C per treatment until the v(CN) stretch was undetectable. The relative strength and position of the v(CN) was used to determine thermal cyano decomposition and link the thermal treatment with the structure of the material. **Figure 7** shows batch 2 at room temperature, as well as after various heat treatments from 170 ^{0}C to 250 ^{0}C. At 190 ^{0}C the v(CN) stretch has increased in strength and decreased in frequency by 6 cm^{-1}. It has also narrowed slightly. This indicates an annealing effect has taken place as the heat removes defects from the structure.
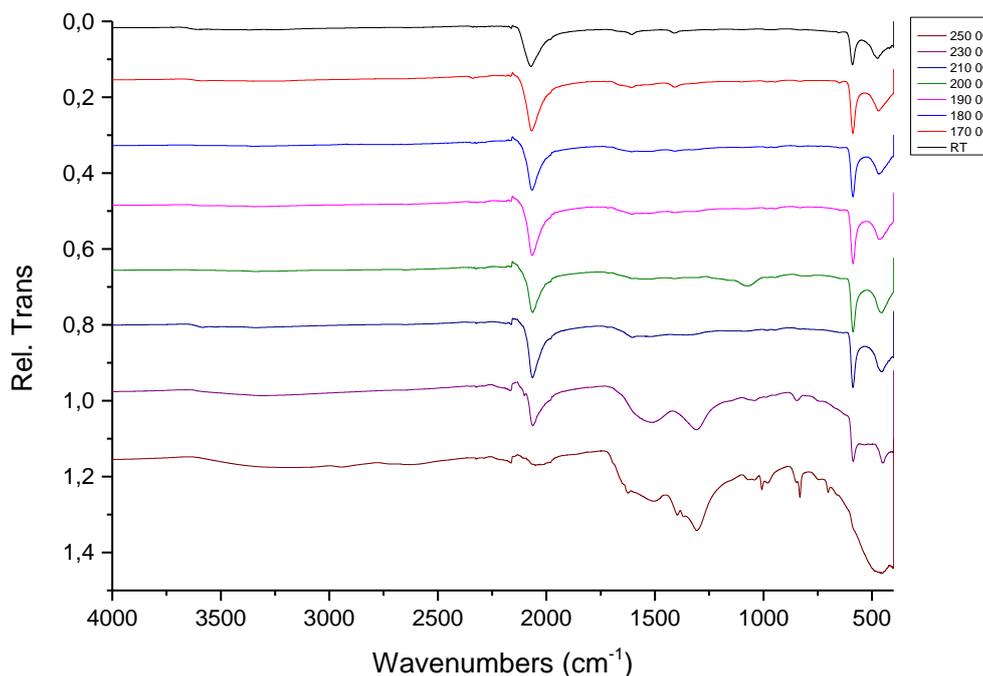
Figure 7: FT-IR of batch 2 at room temperature, as well as after various heat treatments from 170 0C to 250 0C. Each scan corresponds to 4 hours at that temperature. The sample is the same one throughout the experiment.

This continues up to 210 ^{0}C. However, at 230 ^{0}C the peak begins to decrease in strength, although it is still well structured. At 250 ^{0}C the peak has broken down. The beginnings of KOCN (2,160 cm^{-1} and 1,300 cm^{-1}) and carbonate humps (1,400-1,700 cm^{-1}) are clearly present at 190 ^{0}C but become more and more noticeable as the temperature is increased, eventually dominating the spectra by 250 ^{0}C.[38]

In batch 3 (**Figure 8)** we initially see the same annealing effect when the batch is heated in air. However, it does not last and as suggested previously by the TGA measurement the material begins to break down at much lower temperatures than batch 2. When the sample is heated above 170 ^{0}C an almost 80 % break down in the intensity of the v(CN) stretch is observed. No signal is observable in the M-L region. The KOCN peaks disappear at 190°C and a weak Cu-HCF (III) v(CN) stretch appears. At 200^{0}C the CN ligand peaks have completely broken down.
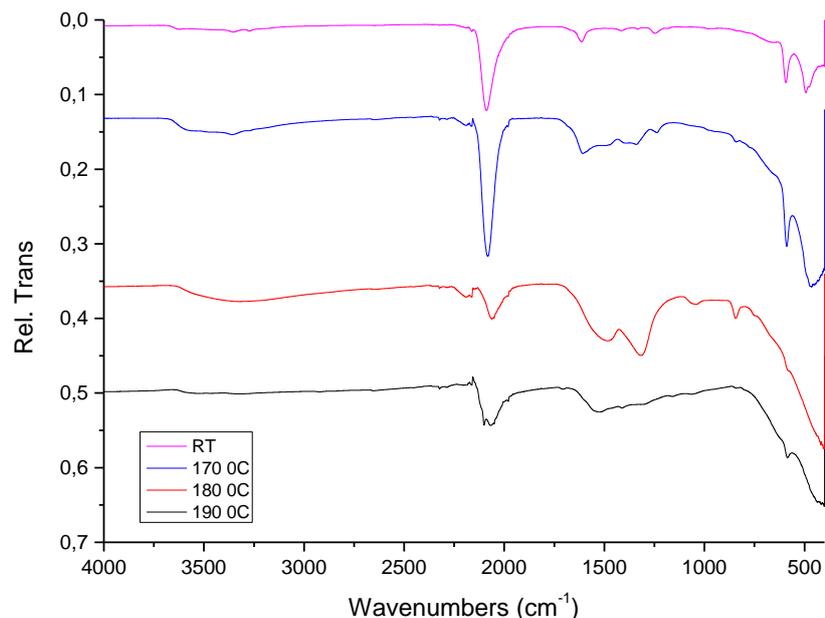
Figure 8: FT-IR of batch 3 at room temperature, as well as after various heat treatments from 170 ^{0}C to 250 ^{0}C..

Finally, looking at batch 4, when it was heated to 170 ^{0}C 75% of the intensity of the v(CN) stretch was lost, (**Figure 9**). It has decreased in frequency by almost 30 cm-1 but has also broadened. Also a peak at 2,180 cm^{-1} is now present indicating the presence of Cu-HCF (III). KOCN forms at 170 °C. By 180 ^{0}C the Cu-HCF (III) v(CN) peak has disappeared and the Cu-HCF (II) stretch is almost gone.

Gathering these results together we see that depending on the particle stoichiometry (Cu:Fe ratio) it is possible to synthesis Cu-HCF where the cyano groups decompose at 180 °C, 190 °C or 250 °C. The lower resistance to heat shown by batch 4 when compared to batches 3 and 2, and of batch 3 when compared to batch 2 (**Figure 7-9**) is assumed to be due to the ever increasing structural water content moving from batch 2 to 4. As water becomes more and more an integral part of the Cu-HCF structure the material becomes more susceptible to thermal decomposition through water loss. The ever increasing structural dependence of Cu-HCF on water is highlighted in the graphic in **Figure 5**.
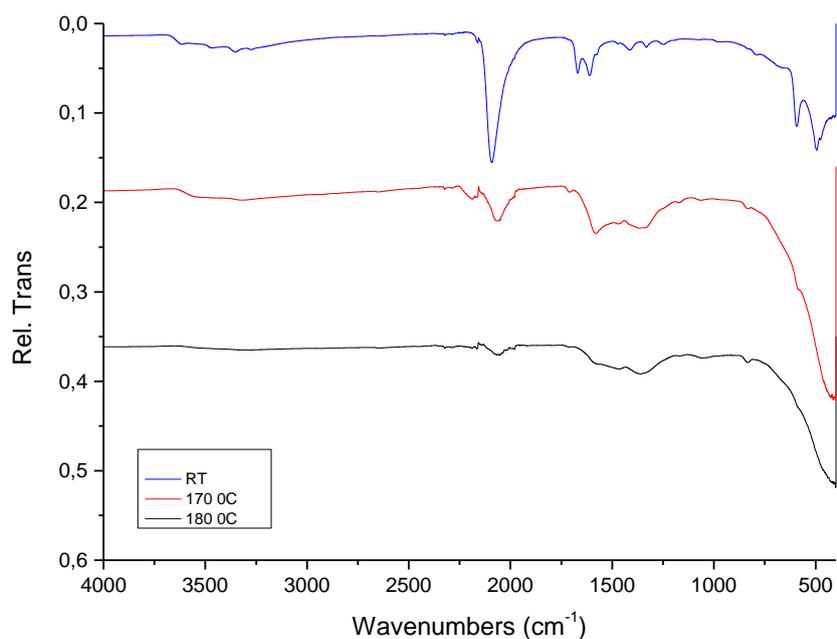
Figure 9: FT-IR of batch 4 at room T (blue) and after heating at 170 °C (red) and 180°C (black). the v(CN) stretch has decreased in strength by 75 %.

4. Impact of the nature of the guest ion (K or Cs) on thermal stability

Finally, the previously described FT-IT thermal studies were carried out on each batch after the K^+ guest ion was exchanged for Cs^+. The Cs^+ sorption behaviour of these samples followed closely what has previously been reported by Takahashi et al; [7] kinetic and isotherm data is available in the SI. The study showed an increase in the thermal stability of the cyano ligand throughout the series after Cs^+ was introduced into the structure. Batches 2, 3 and 4 saw a 20 °C, 50 °C and 40 °C increase respectively. Focusing on batch 3, (**Figure 10**) EA of the exchanged sample showed no change in the Cu to Fe ratio loss during Cs/K exchange. This indicates that there is no difference in the number of Fe vacancies after guest ion exchange and there is also no change in the amount of structural water present.
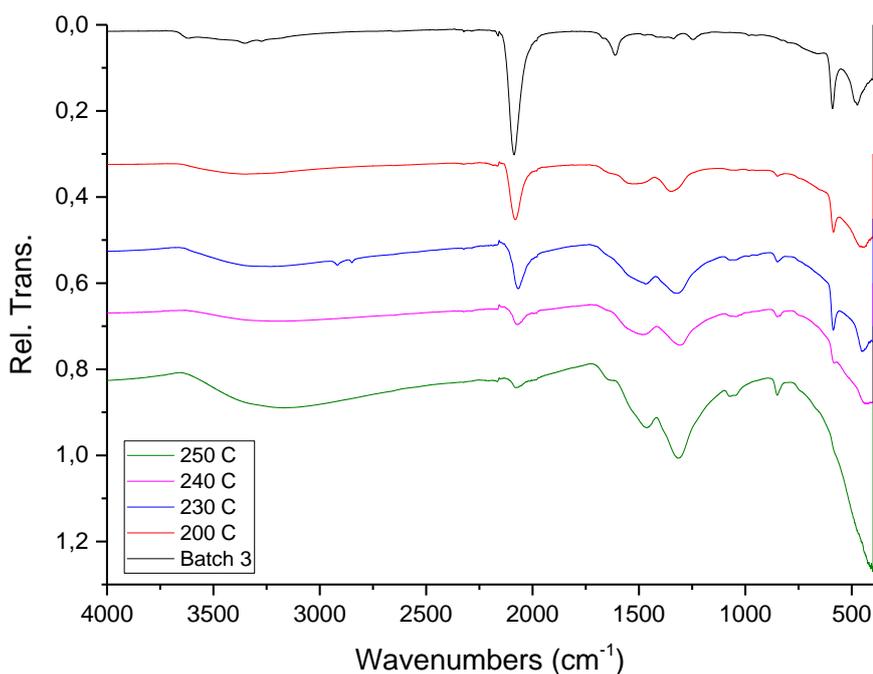
Figure 10: FT-IR of Cs exchanged batch 3 taken before thermal treatment began (black) and after thermal treatment at 200, 230, 240 and 250°C.

However, we believe that the presence of Cs^+ is indirectly responsible for the change in thermal stability as reported in Figure 10. v(CN) and M-L stretches are now stable and structured to 230 °C. A weak v(CN) is still visible up to 250 °C. This is an increase of 50 °C when compared with the batch 3 before Cs/K exchange. An explanation can be found in the metal-ligand region of the FT-IR spectra. As previously shown in **Figure 3** there are two distinct Cu regions present in each batch. The literature has attributed this to the presence of a Jahn-Teller distortion within these materials.[37] When Cs is added to each batch we see a change in this region with an inversion of the relative intensities of the v(Cu-N) stretches, (**Figure 11 and SI**). The re-organisation of these stretches demonstrates a change in the degree of the copper centres Jahn-Teller distortion. That is the copper ligand bonds are lengthening (or shortening) after Cs is introduced. We believe that the Cu-O bonds are shortening and strengthening after Cs is introduced into matrix. As reported M^+ guest ions are thought to interact with copper hexacyanoferrate structural water.[25] Separately, as noted by Mähler et al. hydrated potassium $K(OH_2)_7$ has a K-O distance of 2.81 Å while hydrated caesium, $Cs(OH_2)_8$, shows a much weaker interaction with water possessing a Cs-O bond length of 3.081 Å.
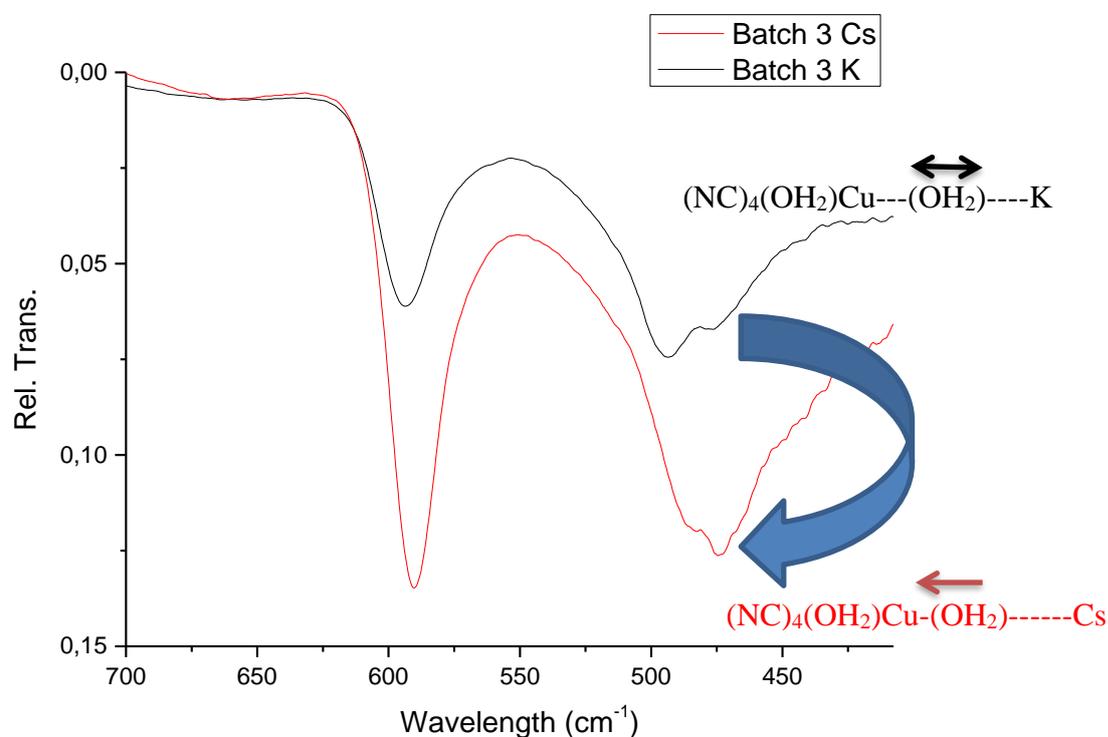
Figure 11: FT-IR of batch 3 before (black) and after (red) Cs/K exchange. Note the inversion of the relative strength of the v(Cu-N) stretches.

By exchanging the K^+ guest ion for an ion with a significantly lower hydration energy and a weaker hydration shell (in this case Cs^+) the copper is able to increase its hold on the partially shared structural water molecule. This in turn causes the Cu-O bonds to shorten and strengthen. [25-26,27,] That is, the weaker the structural waters interaction with the guest ion, the stronger it will be with the copper. This strengthening of the bond between the copper and the structural water is what leads to an increase in thermal stability. Another possible explanation could be due to the stronger interaction of the larger Cs^+ ions with the cyano ligands, relative to that of the smaller K^+ ions.[36] Enhanced guest ion interaction with the cyano ligands has been seen to coincide with a lengthening of the Cu-N, and subsequent shortening of the Cu-O bonds.[25] Again this leads to the same conclusion, a stronger Cu-O bond.

Conclusions

Here we report the tuning of the thermal stability of Cu-HCF nanoparticles by varying the Cu to Fe reactant ratio. Elemental analysis showed it was possible to tune the Fe to Cu ratio and therefore the structural water content of the particles. This allowed us to alter the thermal sensitivity of the material. The nature of the guest ion was also shown to affect the decomposition temperature. The presence of Cs was seen to cause a change in the Cu co-ordination sphere as seen in FT-IR. As no change in the Fe to Cu ratio was detected this improved stability is believed to be a change in the degree of the Jahn-Teller distortion present in Cu-HCF. The next step is to perform a full structural analysis of the material before and after Cs exchange. This is currently been undertaken.

Author Information

Corresponding Author

Agnès Grandjean, CEA, DEN, Univ. Montpellier, DE2D, SEAD, Laboratory of Supercritical and Decontamination Processes, F-30207 Bagnols-sur-Cèze, France.

E-mail: agnes.grandjean@cea.fr

Author Contributions

The manuscript was written through contributions of all authors. All authors have given approval to the final version of the manuscript.

Funding Sources

Acknowledgements

References

1.   Tao, Q. Q.; Zhang, X.; Prabaharan, K.; Dai, Y., Separation of cesium from wastewater with copper hexacyanoferrate film in an electrochemical system driven by microbial fuel cells. *Bioresour. Technol.* **2019,** *278*, 456-459.

2.   Roh, H.; Kim, Y.; Kim, Y. K.; Harbottle, D.; Lee, J. W., Amino-functionalized magnetic chitosan beads to enhance immobilization of potassium copper hexacyanoferrate for selective Cs+ removal and facile recovery. *RSC Adv.* **2019,** *9* (2), 1106-1114.

3.   Wang, J. L.; Zhuang, S. T.; Liu, Y., Metal hexacyanoferrates-based adsorbents for cesium removal. *Coord. Chem. Rev.* **2018,** *374*, 430-438.

4.   Causse, J.; Tokarev, A.; Ravaux, J.; Moloney, M.; Barre, Y.; Grandjean, A., Facile one-pot synthesis of copper hexacyanoferrate nanoparticle functionalised silica monoliths for the selective entrapment of Cs-137. *J. Mater. Chem. A* **2014,** *2* (25), 9461-9464.

5.   Grandjean, A.; Delchet, C.; Causse, J.; Barré, Y.; Guari, Y.; Larionova, J., Effect of the chemical nature of different transition metal ferrocyanides to entrap Cs. *Journal of Radioanalytical and Nuclear Chemistry* **2016,** *307* (1), 427-436.

6.   Chang, S. Q.; Chang, L.; Han, W.; Li, Z.; Dai, Y. D.; Zhang, H. Q., In situ green production of Prussian blue/natural porous framework nanocomposites for radioactive Cs+ removal. *Journal of Radioanalytical and Nuclear Chemistry* **2018,** *316* (1), 209-219.

7.   Takahashi, A.; Tanaka, H.; Minami, K.; Noda, K.; Ishizaki, M.; Kurihara, M.; Ogawa, H.; Kawamoto, T., Unveiling Cs-adsorption mechanism of Prussian blue analogs: Cs+-percolation via vacancies to complete dehydrated state. *RSC Adv.* **2018,** *8* (61), 34808-34816.

8.   Cabaud, C.; Barré, Y.; De Windt, L.; Gill, S.; Dooryhée, E.; Moloney, M. P.; Massoni, N.; Grandjean, A., Removing Cs within a continuous flow set-up by an ionic exchanger material transformable into a final waste form. *Adsorption* **2019**.

9.   Moloney, M. P.; Cabaud, C.; Massoni, N.; Stafford, S.; Gun'ko, Y. K.; Venkatesan, M.; Grandjean, A., Searching for the nano effect in Cu-HCF (II) particles to improve Cs sorption efficiency: Highlighting the use of intrinsic magnetism. *Colloids and Surfaces A: Physicochemical and Engineering Aspects* **2019,** *582*, 123758.

10.   Cabaud, C.; Barré, Y.; De Windt, L.; Gill, S.; Dooryhée, E.; Moloney, M. P.; Massoni, N.; Grandjean, A., Removing Cs within a continuous flow set-up by an ionic exchanger material transformable into a final waste form. *Adsorption* **2019,** *25* (4), 765-771.

11.   Zong, Y.; Zhang, Y.; Lin, X.; Ye, D.; Qiao, D.; Zeng, S., Facile synthesis of potassium copper ferrocyanide composite particles for selective cesium removal from wastewater in the batch and continuous processes. *RSC Adv.* **2017,** *7* (50), 31352-31364.

12.   Hwang, K. S.; Park, C. W.; Lee, K. W.; Park, S. J.; Yang, H. M., Highly efficient removal of radioactive cesium by sodium-copper hexacyanoferrate-modified magnetic nanoparticles. *Colloid Surf. A-Physicochem. Eng. Asp.* **2017,** *516*, 375-382.

13.   Kim, Y. K.; Kim, T.; Kim, Y.; Harbottle, D.; Lee, J. W., Highly effective Cs+ removal by turbidity-free potassium copper hexacyanoferrate-immobilized magnetic hydrogels. *J. Hazard. Mater.* **2017,** *340*, 130-139.

14.   Kim, Y. K.; Bae, K.; Kim, Y.; Harbottle, D.; Lee, J. W., Immobilization of potassium copper hexacyanoferrate in doubly crosslinked magnetic polymer bead for highly effective Cs+ removal and facile recovery. *J. Ind. Eng. Chem.* **2018,** *68*, 48-56.

15.   Motl, A.; John, J.; Sebesta, F., Composite absorbers of inorganic ion-exchangers and polyacrylonitrile binding matrix - V. Influence of ionising radiation on the leachability of Cs-137 from cemented composite NiFC-PAN absorber. *Journal of Radioanalytical and Nuclear Chemistry* **1997,** *222* (1-2), 205-207.

16.   Michel, C.; Barré, Y.; De Windt, L.; de Dieuleveult, C.; Brackx, E.; Grandjean, A., Ion exchange and structural properties of a new cyanoferrate mesoporous silica material for Cs removal from natural saline waters. *Journal of Environmental Chemical Engineering* **2017,** *5* (1), 810-817.

17.   Catala, L.; Mallah, T., Nanoparticles of Prussian blue analogs and related coordination polymers: From information storage to biomedical applications. *Coord. Chem. Rev.* **2017,** *346*, 32-61.

18.   Mayer, M.; Dedovets, D.; Guari, Y.; Larionova, J.; Long, J.; Causse, J., Synthesis of poly(diallyldimethylammonium) capped copper hexacyanoferrate (CuHCF) nanoparticles: An efficient stabiliser for Pickering emulsions. *J. Colloid Interface Sci.* **2017,** *505*, 364-372.

19.   Boles, M. A.; Ling, D.; Hyeon, T.; Talapin, D. V., The surface science of nanocrystals. *Nat. Mater.* **2016,** *15* (2), 141-153.

20.   Yoffe, A. D., Semiconductor quantum dots and related systems: electronic, optical, luminescence and related properties of low dimensional systems. *Adv. Phys.* **2001,** *50* (1), 1-208.

21.   Rajesh, K. M.; Ajitha, B.; Ashok Kumar Reddy, Y.; Suneetha, Y.; Sreedhara Reddy, P., Synthesis of copper nanoparticles and role of pH on particle size control. *Materials Today: Proceedings* **2016,** *3* (6), 1985-1991.

22.   Guardia, P.; Labarta, A.; Batlle, X., Tuning the Size, the Shape, and the Magnetic Properties of Iron Oxide Nanoparticles. *The Journal of Physical Chemistry C* **2011,** *115* (2), 390-396.

23.   Hu, M.; Chen, J. Y.; Li, Z. Y.; Au, L.; Hartland, G. V.; Li, X. D.; Marquez, M.; Xia, Y. N., Gold nanostructures: engineering their plasmonic properties for biomedical applications. *Chem. Soc. Rev.* **2006,** *35* (11), 1084-1094.

24.   Moloney, M. P.; Gun'ko, Y. K.; Kelly, J. M., Chiral highly luminescent CdS quantum dots. *Chem. Commun.* **2007,** (38), 3900-3902.

25.   Wardecki, D.; Ojwang, D. O.; Grins, J.; Svensson, G., Neutron Diffraction and EXAFS Studies of K2x/3Cu[Fe(CN)6]2/3·nH2O. *Crystal Growth & Design* **2017,** *17* (3), 1285-1292.

26.   Tachikawa, H.; Haga, K.; Yamada, K., Mechanism of K+, Cs+ ion exchange in nickel ferrocyanide: A density functional theory study. *Computational and Theoretical Chemistry* **2017,** *1115*, 175-178.

27.   Mähler, J.; Persson, I., A Study of the Hydration of the Alkali Metal Ions in Aqueous Solution. *Inorganic Chemistry* **2012,** *51* (1), 425-438.

28.   Gotoh, A.; Uchida, H.; Ishizaki, M.; Satoh, T.; Kaga, S.; Okamoto, S.; Ohta, M.; Sakamoto, M.; Kawamoto, T.; Tanaka, H.; Tokumoto, M.; Hara, S.; Shiozaki, H.; Yamada, M.; Miyake, M.; Kurihara, M., Simple synthesis of three primary colour nanoparticle inks of Prussian blue and its analogues. *Nanotechnology* **2007,** *18* (34), 6.

29.   Akerblom, I. E.; Ojwang, D. O.; Grins, J.; Svensson, G., A thermogravimetric study of thermal dehydration of copper hexacyanoferrate by means of model-free kinetic analysis. *Journal of Thermal Analysis and Calorimetry* **2017,** *129* (2), 721-731.

30.   Soek, R. N.; Schmidt, A.; Winnischofer, H.; Vidotti, M., Anisotropic behavior of layer-by-layer films using highly disordered copper hexacyanoferrate(II) nanoparticles. *Appl. Surf. Sci.* **2016,** *378*, 253-258.

31.   Ojwang, D. O.; Grins, J.; Wardecki, D.; Valvo, M.; Renman, V.; Häggström, L.; Ericsson, T.; Gustafsson, T.; Mahmoud, A.; Hermann, R. P.; Svensson, G., Structure Characterization and Properties of K-Containing Copper Hexacyanoferrate. *Inorganic Chemistry* **2016,** *55* (12), 5924-5934.

32.   Avila, M.; Reguera, L.; Rodríguez-Hernández, J.; Balmaseda, J.; Reguera, E., Porous framework of T2[Fe(CN)6]·xH2O with T=Co, Ni, Cu, Zn, and H2 storage. *Journal of Solid State Chemistry* **2008,** *181* (11), 2899-2907.

33.   Jiménez-Gallegos, J.; Rodríguez-Hernández, J.; Yee-Madeira, H.; Reguera, E., Structure of Porous Copper Prussian Blue Analogues: Nature of Their High H2 Storage Capacity. *The Journal of Physical Chemistry C* **2010,** *114* (11), 5043-5048.

34.   Gil, D. M.; Avila, M.; Reguera, E.; Pagola, S.; Inés Gómez, M.; Carbonio, R. E., Lead hexacyanoferrate(II) tetrahydrate: Crystal structure, FTIR spectroscopy and thermal decomposition studies. *Polyhedron* **2012,** *33* (1), 450-455.

35.   Ghosh, S. N., Infrared spectra of the Prussian blue analogs. *Journal of Inorganic and Nuclear Chemistry* **1974,** *36* (11), 2465-2466.

36.   Lejeune, J.; Brubach, J.-B.; Roy, P.; Bleuzen, A., Application of the infrared spectroscopy to the structural study of Prussian blue analogues. *Comptes Rendus Chimie* **2014,** *17* (6), 534-540.

37.   Gellings, P. J., Structure of some Hexacyanoferrates (II) of the Type K2MIIFe(CN)6. In *Zeitschrift für Physikalische Chemie*, 1967; Vol. 54, p 296.

38.   De Marco, D.; Marchese, A.; Migliardo, P.; Bellomo, A., Thermal analysis of some cyano compounds. *Journal of thermal analysis* **1987,** *32* (3), 927-937.